

BVRI Photometric Observations, Light Curve Solutions and Orbital Period Analysis of BF Pav

Atila Poro^{1,2}, Fahri Alicavus^{3,4}, Eduardo Fernández-Lajús^{5,6}, Fatemeh Davoudi^{1,2}, PegahSadat MirshafieKhozani¹, Mark G. Blackford⁷, Edwin Budding⁸, Behjat Zarei Jalalabadi¹, Jabar Rahimi¹ and Farzaneh Ahangarani Farahani¹

¹ The International Occultation Timing Association Middle East section, Iran; info@iota-me.com

² Astronomy Department of the Raderon Lab, Burnaby, BC, Canada

³ Çanakkale Onsekiz Mart University, Faculty of Arts and Sciences, Department of Physics, 17020, Çanakkale, Turkey

⁴ Çanakkale Onsekiz Mart University, Astrophysics Research Center and Ulupnar Observatory, 17020, Çanakkale, Turkey

⁵ Instituto de Astrofísica de La Plata (CCT La Plata-CONICET-UNLP), La Plata, Argentina

⁶ Facultad de Ciencias Astronómicas y Geofísicas, Universidad Nacional de La Plata, Paseo del Bosque, B1900FWA, La Plata, Argentina

⁷ Variable Stars South (VSS), Congarinni Observatory, Congarinni, NSW, 2447, Australia

⁸ Carter Observatory, 40 Salamanca Rd, Kelburn, Wellington 6012, New Zealand

Received 2020 September 9; accepted 2021 February 19

Abstract A new ephemeris, period change analysis and light curve modeling of the W UMA-type eclipsing binary BF Pav are presented in this study. Light curves of the system taken in *BVRI* filters from two observatories, in Australia and Argentina, were modeled using the Wilson-Devinney code. The results of this analysis demonstrate that BF Pav is a contact binary system with a photometric mass ratio $q = 1.460 \pm 0.014$, a fillout factor $f = 12.5\%$, an inclination of 87.97 ± 0.45 deg and a cold spot on the secondary component. By applying the distance modulus formula, the distance of BF Pav was calculated to be $d = 268 \pm 18$ pc which is in good agreement with the Gaia EDR3 distance. We obtain an orbital period increase at a rate of 0.142 s century⁻¹ due to a quadratic trend in the $O - C$ diagram. Also, an alternative sudden period jump probably occurred which could be interpreted as a rapid mass transfer from the lower mass star to its companion of about $\Delta M = 2.45 \times 10^{-6} M_{\odot}$. Furthermore, there is an oscillatory behavior with a period of 18.3 ± 0.3 yr. Since BF Pav does not seem to have significant magnetic activity, this behavior could be interpreted as the light-time effect caused by an undetected third body in this system. In this case, the probability for the third body to be a low mass star with $M \geq 0.075 M_{\odot}$ or a brown dwarf is 5.4% and 94.6% respectively. If we assume $i' = 90^{\circ}$, $a_3 = 8.04 \pm 0.33$ AU. The mass of the secondary component was also determined following two different methods which result close to each other.

Key words: techniques: photometric — binaries: eclipsing — stars: individual (BF Pav)

1 INTRODUCTION

W UMA-type binary systems have short orbital periods of less than a day and they exhibit continuous light variations (Dryomova & Svechnikov 2006). These systems are abundant in binary stars (Okamoto & Sato 1970). They include two stars usually surrounded by a common envelope resulting from mass overflowing from the Roche lobe of one binary component (Smith 1984). Despite many studies that have been done on the basis of a

Common Connective Envelope (CCE) in recent years (Qian et al. 2018), many details are still undetermined about the evolutionary state of contact binaries due to extreme spectral line broadening for achieving spectra analysis (Yang & Qian 2015). For justifying the contact phase in contact binaries, Stępień (2006) suggested angular momentum loss through magnetic wind, whereas Qian et al. (2018) proposed transmission of a large amount of angular momentum to a third body. So, it is efficient to investigate the formation and structure of W UMA-type

contact binaries for studying physical processes in these systems in more detail. We can find valuable details about mass transfer, mass loss and also the evolutionary state of close binaries by perusing their orbital variations.

The BF Pav binary system, which is located in the constellation of Pavo in the Southern Hemisphere, is a W UMa-type variable star with an approximate period of 0.30231864 d and G8 spectral type (Gonzalez et al. 1996). Its apparent magnitude in the *V*-band is 12.17 (APASS9). The variability of BF Pav was discovered by Shapley & Mohr (1940) in 1939 and the first photoelectric light curve was obtained by Hoffmann (1981). Although these observations did not cover the complete orbital period, the observer derived a period of 0.3056 d (Gonzalez et al. 1996). Between 1987 and 1993, BF Pav was observed photoelectrically in *UBV* filters in the observational program of Southern Short-Period Eclipsing Binaries to determine the times of minima, and photometric and absolute parameters. The photometric solution resulted in a mass ratio of $q = 1.4 \pm 0.2$, a fillout factor equal to 10% and efficient thermal contact between the components, $\Delta T = 100$ K (Gonzalez et al. 1996). Dryomova & Svechnikov (2006) found the rate of period change of BF Pav to be $\dot{p} = 1.62 \times 10^{-7}$ d yr⁻¹ in their study by checking the variation in the orbital period of W Uma-type contact systems. Zhang et al. (2015) noted that BF Pav has a similar period increase to GK Aqr.

In this paper, we present a new ephemeris based on our observations as well as new period change analysis and light curve solutions to investigate the evolutionary state of BF Pav in more detail.

2 OBSERVATION AND DATA REDUCTION

The observation of BF Pav was carried out in September 2017, April 2018, August and June 2019, and July 2020, and a total of 3517 images were taken during eight nights; 2054 images were acquired with a 14-inch Ritchey-Chretien telescope and SBIG STT3200-ME CCD equipped with Astrodon Johnson-Cousins *BVRI* filters at the Congarinni Observatory which is located in Australia with geographical coordinates 152°52′ East and 30°44′ South and 20 meters above the mean sea level. Each frame was recorded at 2×2 binning with 50 s exposure time in each filter and CCD temperature set at -15° C. Another 1463 images were taken with the 2.15 m “Jorge Sahade” telescope at the Complejo Astronomico El Leoncito (CASLEO) Observatory (69°18′W, 31°48′S 2552 m above sea level), Argentina. A VersArray 2048B, Roper Scientific cryogenic CCD and a *V*-band filter were employed. Each frame was recorded at 5×5 binning with 15 s exposure time.

GSC 8770–1511 was chosen as a check star and eight stars were selected as comparison stars with appropriate apparent magnitude in comparison to BF Pav. The general characteristics of BF Pav with the comparisons and the check star are shown in Table 1.

Standard procedures for CCD image processing (aligned pictures, bias and dark removal, flat-fielding to correct for vignetting, and pixel-to-pixel variations) were applied. We did all image processing and plotting raw images with MaxIm DL software (George 2000). Then more modifications were made with AstroImageJ (AIJ) software (Collins et al. 2017). AIJ is a powerful tool for astronomical image analysis and precise photometry (Davoudi et al. 2020).

We determined 11 primary and 8 secondary minimum times from the observed light curves in *BVRI* filters. These minima were calculated by following the Kwee & van Woerden (1956) method.

3 ORBITAL PERIOD VARIATIONS

Considering 58 mid-eclipse times including 30 primary and 28 secondary eclipses from the previous study and our observations, we analyzed the orbital period variation of this system. We averaged all the times of minima from literature and our observations that were in the same filter at the same time. All times of minima are expressed in Barycentric Julian Date in Barycentric Dynamical Time BJD_{TDB} and listed in Table 2. It includes errors, epochs, $O-C$ values and the references of mid-eclipse times in the last column. The linear ephemeris of Gonzalez et al. (1996) was referenced for computing epochs and the $O-C$ values,

$$\begin{aligned} \text{Min.}I(BJD_{\text{TDB}}) &= 2448056.9014 \pm (0.0002) \\ &+ 0.30231864(\pm 0.00000007) \times E. \end{aligned} \quad (1)$$

To proceed with analysis of the behavior of the period, we first averaged all the minimum times of Table 2 that correspond to the same event, in such a way that they do not have an overestimated weight in the adjustments. In the cases where an estimate of error was not reported in the original references, we assumed the error to be the order of its last significant digit. Then, a first quadratic fitting applying the least-squares method was done, using the errors to weight each data point properly considering $W = (\frac{1}{\text{err}^2})$. The following ephemeris formula was obtained,

$$\begin{aligned} \text{Min.}I(BJD_{\text{TDB}}) &= (2448056.90186 \pm 0.00027) \\ &+ (0.30231846 \pm 5.0 \times 10^{-8}) \times E \\ &+ ((6.8 \pm 1.5) \times 10^{-12}) \times E^2 [\text{d}] \end{aligned} \quad (2)$$

where E is the cycle number after the reference cycle. The rate of change of the binary period is given by the quadratic

Table 1 Characteristics of the *Variable star*, *Check star* and *Comparison stars* (from: SIMBAD^a and APASS9^b)

Star type	Star name	RA. (J2000)	DEC. (J2000)	Magnitude (V)
<i>Variable</i>	BF Pav	18 45 39.32	−59 38 25.87	12.17
<i>Comparison</i> ₁	GSC 8770–1107	18 45 30.01	−59 32 34.9	12.23
<i>Comparison</i> ₂	GSC 8770–1582	18 45 50.08	−59 36 59.1	13.43
<i>Comparison</i> ₃	GSC 8770–1663	18 45 49.66	−59 37 48.9	13.43
<i>Comparison</i> ₄	GSC 8770–0085	18 45 33.39	−59 39 50.5	13.52
<i>Comparison</i> ₅	GSC 8770–103	18 46 0.36	−59 36 5.8	12.18
<i>Comparison</i> ₆	GSC 8770–1383	18 45 42.38	−59 32 5.3	13.39
<i>Comparison</i> ₇	GSC 8770–1325	18 45 18.25	−59 44 27.2	13.23
<i>Comparison</i> ₈	GSC 8770–1333	18 45 56.89	−59 40 26.6	13.54
<i>Check</i>	GSC 8770–1511	18 45 32.73	−59 36 25.0	13.48

^a: <http://simbad.u-strasbg.fr/simbad/>; ^b: <http://vizier.u-strasbg.fr/viz-bin/>.

Table 2 Available Times of Minima for BF Pav

<i>Min.</i> (<i>BJD</i> _{TDB})	Error	Epoch	<i>O</i> − <i>C</i>	References
2444438.7617		−11968	0.0098	Hoffmann 1981
2445886.4094	0.0001	−7179.5	0.0047	Spencer Jones 1988
2445886.5621	0.0004	−7179	0.0062	Spencer Jones 1988
2446936.8129		−3705	0.0021	Gonzalez et al. 1996
2447259.8388		−2636.5	0.0005	Gonzalez et al. 1996
2447368.6721		−2276.5	−0.0009	Gonzalez et al. 1996
2448056.7488		−0.5	−0.0014	Gonzalez et al. 1996
2448056.9009		0	−0.0005	Gonzalez et al. 1996
2448056.9014	0.0002	0	0.0000	Gonzalez et al. 1996
2448057.8076		3	−0.0008	Gonzalez et al. 1996
2448058.8660		6.5	−0.0005	Gonzalez et al. 1996
2449182.736		3724	0.0000	Gonzalez et al. 1996
2449184.7009		3730.5	−0.0002	Gonzalez et al. 1996
2449217.5031		3839	0.0004	Gonzalez et al. 1996
2449217.6548		3839.5	0.0010	Gonzalez et al. 1996
2449218.5615		3842.5	0.0007	Gonzalez et al. 1996
2449219.6190		3846	0.0001	Gonzalez et al. 1996
2452404.5462	0.0001	14381	0.0004	Zakrzewski (ASAS-3)
2452404.6964	0.0002	14381.5	−0.0005	Zakrzewski (ASAS-3)
2453479.4393	0.0005	17936.5	−0.0004	Zakrzewski (ASAS-3)
2453558.4955	0.0004	18198	−0.0005	Zakrzewski (ASAS-3)
2454606.9368	0.0003	21666	−0.0003	Zakrzewski (ASAS-3)
2454614.9485	0.0001	21692.5	0.0000	Zakrzewski (ASAS-3)
2454778.6540	0.0001	22234	0.0000	Zakrzewski (Catalina)
2454921.4991	0.0002	22706.5	−0.0005	Zakrzewski (Catalina)
2457172.7180	0.0004	30153	0.0026	Juryšek et al. 2017
2458015.5829	0.0001	32941	0.0032	This study
2458227.8106	0.0001	33643	0.0032	This study
2458639.7184	0.0001	35005.5	0.0018	This study
2458639.8699	0.0004	35006	0.0022	This study
2458701.9957	0.0010	35211.5	0.0015	This study
2458702.1472	0.0010	35212	0.0018	This study
2458710.9145	0.0010	35241	0.0019	This study
2458711.0654	0.0010	35241.5	0.0016	This study
2458713.9379	0.0001	35251	0.0021	This study
2458714.0884	0.0001	35251.5	0.0015	This study
2458716.9609	0.0001	35261	0.0019	This study
2458717.1116	0.0001	35261.5	0.0015	This study
2459060.9991	0.0002	36399	0.0015	This study

Eight unpublished minimum times were provided by B. Zakrzewski and were determined from ASAS-3 and Catalina Sky Survey data, according to the Timing Database at Krakow (Kreiner 2004).

coefficient “*Q*” of Equation (2), as follows,

$$\frac{dp}{dE} = 2Q. \quad (3)$$

$\frac{dp}{dE} = (3.6 \pm 0.3) \times 10^{-12} \text{ d cycle}^{-1}$ which represents a continuous period increase at a rate of $(16.4 \pm 3.6) \times 10^{-8} \text{ d yr}^{-1}$ or $0.142 \text{ s century}^{-1}$. Figure 1 displays the

O − *C* diagram calculated using Equation (2) and the residuals of the fitting. The solid black line represents the quadratic least-squares fit to the *O* − *C* values.

As can be seen from Figure 1, the residuals are still quite large, and they do not seem to be randomly distributed. We also note that the *O* − *C* data points can be represented by two simple straight lines with a break

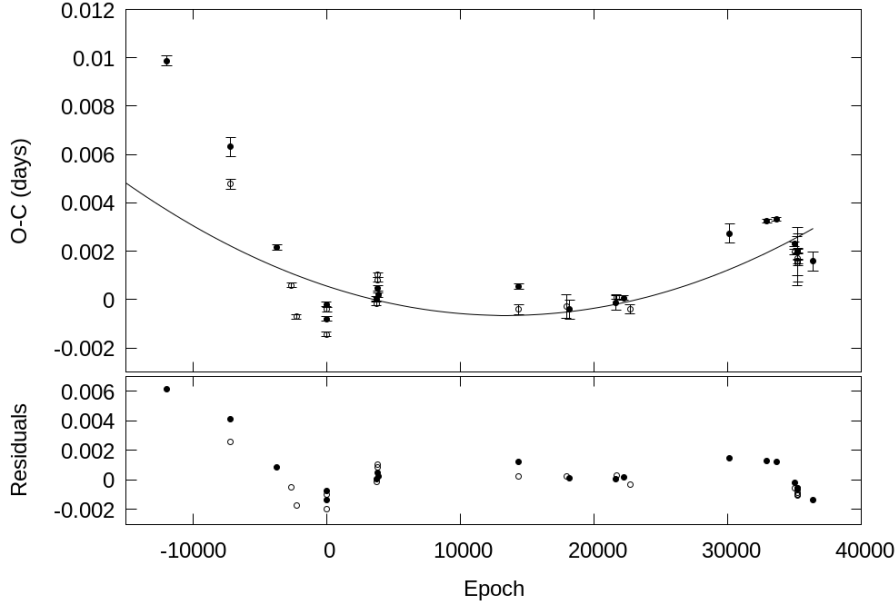


Fig. 1 The quadratic trend in the data points and their residuals. Primary and secondary minima are indicated as filled and open circles respectively.

around $E \sim 0$. The first line, for points with $E < 0.5$, has a steeper downward slope, while a less pronounced ascendant slope is present for $E \geq -0.5$. Proceeding with these linear fittings to each of these branches we obtained the following two ephemerides,

$$\begin{aligned} \text{Min.}I(\text{BJD}_{\text{TDB}}) &= (2448056.89891 \pm 0.00051) \\ &+ (0.30231759 \pm 1.1 \times 10^{-7}) \times E \text{ [d]}, \end{aligned} \quad (4)$$

$$\begin{aligned} \text{Min.}I(\text{BJD}_{\text{TDB}}) &= (2448056.90093 \pm 0.00022) \\ &+ (0.302318713 \pm 9.4 \times 10^{-9}) \times E \text{ [d]}. \end{aligned} \quad (5)$$

Both fittings are depicted in Figure 2. As can be seen at the bottom of that figure, the residuals of the first branch fitting do not show any systematic trend. The sum of squares of the weighted residuals for each linear fitting resulted in 1479 which is less than half of the sum of the weighted residuals of the overall quadratic fitting, 3560, of Equation (2).

Each linear branch would correspond to two different constant period stages, indicating that a sudden period jump should have occurred at $E_c = 1798.75 \sim -1800$ (i.e. JD 2447513 \sim mid Dec. 1988).

The differences between the periods of Equations (4) and (5) give us the period jump which yields $\Delta P = 1.12 \times 10^{-6} \pm 1.1 \times 10^{-7}$ d. This period increase could be interpreted as a rapid mass transfer from the lower mass star to its companion. Supposing a conservative mass transfer, the quantity of mass transferred for this period change could be derived utilizing the following expression

(e.g. [Negu & Tessema 2015](#)).

$$\frac{\Delta P}{P} = 3\Delta M \frac{(M_1 - M_2)}{M_1 M_2}. \quad (6)$$

Considering M_1 and M_2 from Table 5 and the system parameters we obtain the transferred mass to be about $\Delta M = 2.45 \times 10^{-6} M_{\odot}$.

A more detailed inspection of the linear fittings of Figure 2 reveals that the data located at $E > E_c$ exhibit an oscillatory behavior around the second branch line. Then, a new adjustment to the residuals between these data and Equation (5) was made by relying on a sinusoidal function, to get

$$\begin{aligned} O - C &= (0.0013 \pm 0.0002) \\ &\times \sin((0.0002838 \pm 5.2 \times 10^{-6}) \\ &\times E + (-0.578 \pm 0.124)) \text{ [d]}. \end{aligned} \quad (7)$$

The addition of Equations (5) and (7) is depicted in the top panel of Figure 2. The residuals of the whole fittings are presented at the bottom of the same Figure. This sinusoidal variation in the $O - C$ diagram of BF Pav displays an amplitude $K = 0.00134 \pm 0.00021$, $d = 115.5 \pm 18.1$ s and a period of $2\pi P / (0.0002838 \times 365.25) = 18.3 \pm 0.3$ yr.

Some hypotheses are commonly used to explain this kind of behavior. If significant magnetic activity is present in one of the binary components, the changes in its inner structure during the magnetic activity cycles can cause a spin-orbital coupling producing the cyclic variation of the orbital period. This is known as the Applegate mechanism ([Applegate 1992](#)). However, as will be discussed later, BF Pav does not seem to have significant magnetic activity.

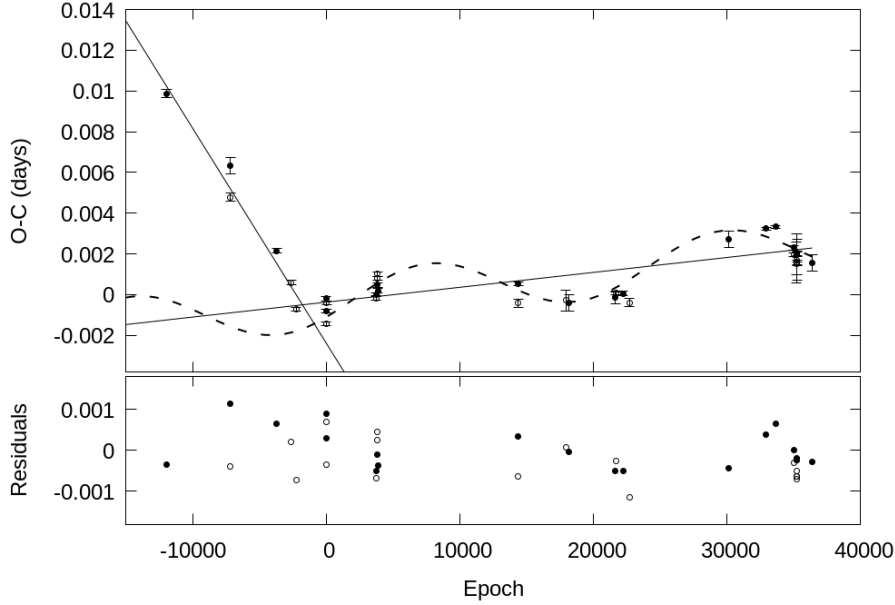


Fig. 2 The two linear ephemeris fittings are represented as solid lines. The dashed line depicts the sinusoidal fitting to the residuals between the data and the linear ephemeris of Eq. (5). In the lower panel, the final residuals after removing the linear trends and the cyclic variation are plotted. Filled and open circles represent primary and secondary minima respectively.

On the other hand, the periodic changes of $O - C$ could also be attributed to the light-time effect, caused by an invisible third body revolving around the binary system (e.g. Irwin 1952). We will restrict our analyses to a circular orbit for the third body because the distribution of points for our collection of times of minima does not deserve a more detailed model with eccentric orbits. In this case, the projected semimajor axis ($a'_{12} \sin i'$) of the orbit of the binary around the barycenter of the triple system is given by

$$a'_{12} \sin i' = K \times c \quad (8)$$

where i' is the inclination of the triple system's orbit, K is the amplitude of the $O - C$ oscillation (Eq. (7)) and c is the speed of light. Thus we obtain $a'_{12} \sin i' = 0.2324 \pm 0.037$ AU. The mass function $f(m)$ must be employed to derive the projected mass of the third body ($M_3 \sin i'$)

$$\begin{aligned} f(m) &= (4\pi^2/GP_3^2)(a'_{12} \sin i')^3 \\ &= (M_3 \sin i')^3 / (M_1 + M_2 + M_3)^2 \end{aligned} \quad (9)$$

where p_3 is the period of oscillation of Equation (6) and G is the gravitational constant.

Thereby, $f(m) = 3.69 \times 10^{-6} \pm 1.75 \times 10^{-6} M_\odot$ and the projected mass $M_3 \sin i' = 0.024 \pm 0.013 M_\odot = 25 \pm 13 M_{\text{Jup}}$. Even inside the errors, the minimum mass for the third body, for the case for $i' = 90^\circ$, is greater or of the order of the lower limit mass for a brown dwarf ($\sim 0.014 M_\odot$).

For an inclination of $i' = 19^\circ$, M_3 would correspond to a star at the lower mass limit of $0.075 M_\odot$. Supposing a uniform distribution of inclination angles, the probability of a star to have certain orbital inclination is given by the distribution function $p(i) = \sin i$. In this way, integrating $p(i)$, we obtain that the probability for the third body to be a low mass star with $M \geq 0.075 M_\odot$ is 5.4%. However, the third body has many more chances to be a brown dwarf with a probability of 94.6%. Using Kepler's third law $a_3[\text{AU}] = (P_3^2[\text{yr}] \times (M_1 + M_2 + M_3)[M_\odot])^{1/3}$ we can derive the semimajor axis of the third body orbit. Supposing an orbital inclination $i' = 90^\circ$, $a_3 = 8.04 \pm 0.33$ AU, which is considerably larger than the common envelope of the binary.

4 LIGHT CURVE ANALYSIS

We utilized the Wilson-Devinney code (W-D, Wilson & Devinney 1971) to analyze the light curves. We preferred to use the W-D code combined with a Monte Carlo simulation to determine the uncertainties of the adjustable parameters (Zola et al. 2004, 2010). The mass ratio of the system could be obtained by the q-search method in the photometric observations, so we did it according to the required standards (Rucinski et al. 2005).

The $(B-V)$ color index is the difference in magnitudes between two wavelength filters B and V . The blue and visual magnitudes are measured through filters centered at 442 nm and 540 nm, respectively. Passing light through

different filters depends on the star's surface temperature according to the Planck Law radiation distributions. It means that by having data from the blue and visual filters we can calculate the $(B-V)$ index and obtain a good estimation of a star's surface temperature (Poro et al. 2021).

The fraction of detected flux of wavelength depends on the telescope mirrors, the bandwidth of filters and the response of the photometer, thus it is necessary to correct our data by calibration with the comparison stars from standard catalogs.

Many studies presented relations between the $(B-V)$ index and the surface temperature of the star such as Code et al. (1976); Sekiguchi & Fukugita (2000) and Ballesteros (2012). Eker et al. (2018) presented relations and tables for different parameters of the main-sequence stars. Eker et al. (2018) selected absolute parameters of 509 main-sequence stars from the components of detached-eclipsing spectroscopic binaries in the solar neighborhood that are used to study Mass-Luminosity (ML), Mass-Radius (MR) and Mass-Temperature (MT) relations. They combined the photometric data of the Sejong Open Cluster Survey (SOS) and typical absolute parameters adjusted from the ML , MR and MT relation functions calibrated in their study. SOS is a photometry project targeting a large number of clusters in the South African Astronomical Observatory (SAAO) Johnson-Cousins $UBVI$ system by Sung et al. (2013).

Based on our data and after calibrating (Høg et al. 2000), we calculated $B-V_{BF\ Pav} = 0^m.803$. As a result, based on Eker et al. (2018), the effective temperature of the secondary component was found to be 5201 K.

Sekiguchi & Fukugita (2000) also derived a $(B-V)$ color-temperature relation. They present T_{eff} as a function of $(B-V)$ color index to represent the metallicity value in four classes. By combining the previous results from Eker et al. (2018) and applying the results of Sekiguchi & Fukugita (2000), the metallicity (Fe/H) value for the primary component of BF Pav can be estimated between -0.75 and -0.25 (star is in population II). As shown in Figure 3, the obtained temperature from derived $(B-V)$ color is also in an acceptable range (4800–5300 K) for the primary component of BF Pav with the method of Sekiguchi & Fukugita (2000).

We assumed gravity-darkening coefficients $g_1 = g_2 = 0.32$ (Lucy 1967), bolometric albedo $A_1 = A_2 = 0.5$ (Ruciński 1969) and linear limb darkening coefficients taken from tables published by van Hamme (1993) in the light curve analysis.

As can be inferred from the light curves, the mean minimum occurred first, and also the temperature of the primary star is higher than the secondary. Based on the unequal minima and the logical light curve solutions, mode

Table 3 Photometric Solutions of BF Pav

Parameter	This study	Gonzales et. al. (1996)
T_1 (K)	5420(6)	5430
T_2 (K)	5201	5330(20)
$\Omega_1 = \Omega_2$	4.394(21)	4.320
i (deg)	87.97(45)	84.8(1.0)
q	1.460(14)	1.4(2)
l_1/l_{tot} (B)	0.471(4)	0.450(30)
l_2/l_{tot} (B)	0.529(5)	0.550
l_1/l_{tot} (V)	0.464(4)	0.445(30)
l_2/l_{tot} (V)	0.536(5)	0.555
l_1/l_{tot} (R)	0.457(4)	
l_2/l_{tot} (R)	0.543(5)	
l_1/l_{tot} (I)	0.450(4)	
l_2/l_{tot} (I)	0.550(5)	
$A_1 = A_2$	0.50	0.5
$g_1 = g_2$	0.32	0.32
f (%)	12.5(3.0)	10
r_1 (back)	0.385(2)	0.386(15)
r_1 (side)	0.349(2)	0.350(15)
r_1 (pole)	0.332(2)	0.334(15)
r_2 (back)	0.452(3)	0.445(15)
r_2 (side)	0.419(3)	0.412(15)
r_2 (pole)	0.395(3)	0.390(15)
r_1 (mean)	0.355(2)	0.355(15)
r_2 (mean)	0.421(3)	0.414(15)
Colatitude _{spot} (deg)	25(4)	
Longitude _{spot} (deg)	120(2)	
Radius _{spot} (deg)	39(2)	
$T_{\text{spot}}/T_{\text{star}}$	0.90(2)	
Phase Shift	-0.0179(1)	

Parameters of a star spot which is on the secondary component.

Table 4 Characteristic Parameters of the Light Curves in the $BVRI$ Filters

Part of LC.	B	V	R	I
MaxI - MaxII	0.032	0.005	0.027	0.011
MaxI - MinI	-1.052	-0.982	-0.920	-0.879
MaxI - MinII	-0.868	-0.820	-0.783	-0.780
MinI - MinII	0.184	0.162	0.137	0.099

3 was chosen for analysis. The parameters obtained from the solutions are given in Table 3. The mean fractional radii of components were calculated with the formula,

$$r_{\text{mean}} = (r_{\text{back}} \times r_{\text{side}} \times r_{\text{pole}})^{1/3}. \quad (10)$$

The observed and synthetic light curves in $BVRI$ filters with residuals are displayed in Figure 4.

Fillout factor is a quantity that indicates the degree of contact in binary star systems defined by Mochnacki & Doughty (1972), and also Lucy & Wilson (1979) that was modified and redefined by Bradstreet (2005),

$$f = \frac{\Omega(L_1) - \Omega}{\Omega(L_1) - \Omega(L_2)} \quad (11)$$

where Ω , $\Omega(L_1)$ and $\Omega(L_2)$ are star surface potential, inner Lagrangian surface potential and outer Lagrangian surface potential, respectively. We calculated a fillout factor of 12.5% with a cold spot from the output parameters of the light curve solutions.

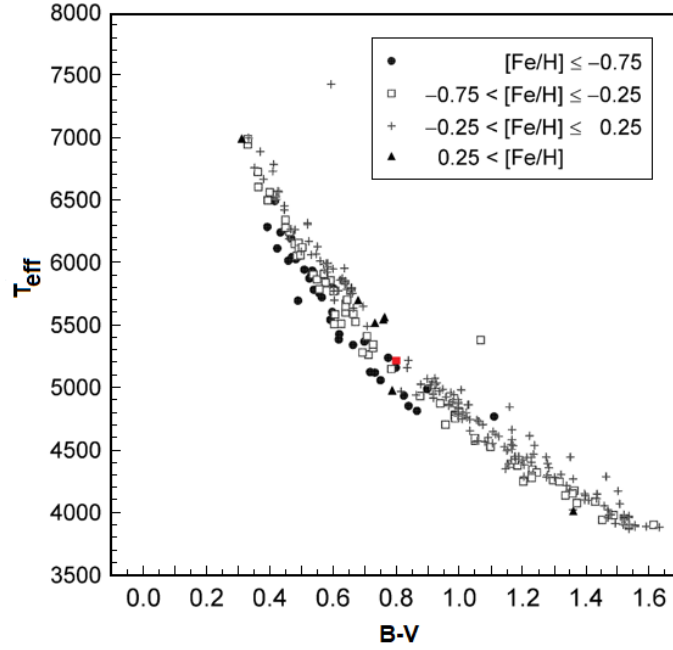


Fig. 3 BF Pav’s position (*red dot*) based on the [Sekiguchi & Fukugita \(2000\)](#) results.

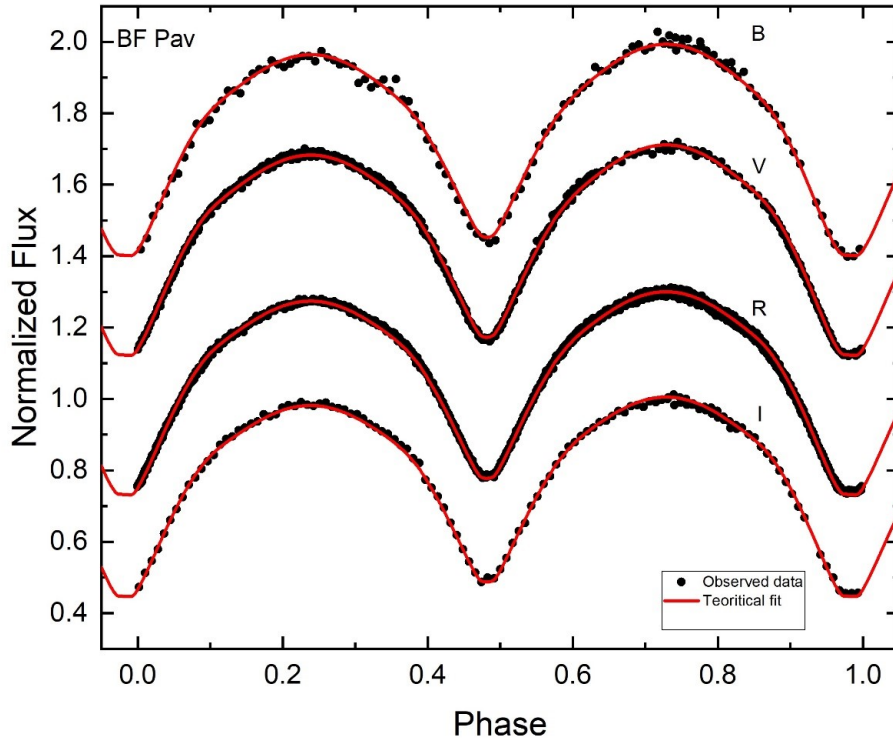


Fig. 4 Observed light curves of BF Pav (*points*) and modeled solutions (*lines*) in the *BVRI* filter from top to bottom, respectively, and residuals are plotted, with respect to orbital phase, shifted arbitrarily in the relative flux.

A difference in the heights of the maxima in light curves of eclipsing binary systems indicates the O’Connell effect ([O’Connell 1951](#)). This binary system appears to demonstrate this effect because we need to add a spot on the secondary component in the light curve solutions.

Table 4 represents the characteristic parameters of the light curves of BF Pav.

$M_{\text{secondary}}$ is derived from a study by [Eker et al. \(2018\)](#) and M is calculated by $q = \frac{M_2}{M_1}$. We also calculated the mass of each component of the binary system following

Table 5 Estimated Absolute Parameters of BF Pav by Two Methods to Calculate the Mass of the Primary Component

Parameter	Eker et al. (2018)		Harmanec (1988)	
	Primary	Secondary	Primary	Secondary
Mass (M_{\odot})	0.626(21)	0.914(32)	0.621(18)	0.906(18)
Radius (R_{\odot})	0.795(8)	0.903(10)	0.792(1)	0.900(1)
Luminosity (L_{\odot})	0.488 (57)	0.534(65)	0.485(57)	0.531(65)
M_{bol} (mag)	5.53(14)	5.43(14)	5.53(14)	5.44(14)
$\log g$ (cgs)	4.43(2)	4.49(2)	4.43(2)	4.49(2)
a (R_{\odot})	2.24(1)		2.23(1)	

the method of Harmanec (1988) who derived a simple approximation formula relating absolute parameters (mass, radius and luminosity) to the effective temperature of the components based on data analysis. For this purpose, we used the following formula,

$$\log \frac{M}{M_{\odot}} = (1.771141X - 21.46965)X + 88.05700)X - 121.6782 \quad (12)$$

where X is $\log(T_{\text{eff}})$. This formula is only defined in the range of $4.62 \geq \log(T_{\text{eff}}) \geq 3.71$ (Harmanec 1988). So, we calculated M_2 as the mentioned range is valid for secondary T_{eff} of BF Pav due to our photometric solution. The absolute parameters are given in Table 5 and there is high conformity between the results which were obtained by two methods.

According to the estimated absolute parameters of this binary system, the distance was calculated. We obtained $m_{\text{system}} = 12.908(25)$ from our light curve and $M_{\nu} = 5.611(29)$ for the secondary component ($BC_1 = -0.181$) from Eker et al. (2018). So, the distance to the binary system is computed from the formula,

$$d(\text{pc}) = 10^{\left(\frac{m_{\text{system}} - M_{\nu} + 5 - A_{\nu}}{5}\right)}. \quad (13)$$

Therefore, an estimate of the distance of this binary system is 268 ± 18 parsec using $A_{\nu} = 0.155$ (Schlafly & Finkbeiner (2011)). The three-dimensional view of BF Pav and the Roche lobe configuration of BF Pav are illustrated in Figure 5.

5 RESULT AND CONCLUSION

The photometric observations of BF Pav were carried out during eight nights utilizing *BVRI* filters. This study's approach is to present a new ephemeris and light curve analysis of the W UMa type eclipsing binary BF Pav and probe this binary system's period changes.

According to a quadratic trend in the $O - C$ diagram, we obtain a period increase at a rate of $(16.4 \pm 3.6) \times 10^{-8} \text{ d yr}^{-1}$ or $0.142 \text{ s century}^{-1}$, but probably a sudden period jump of $\Delta P = 1.1 \times 10^{-7} \text{ d}$ could have occurred instead at $E_c=1800$. This period increase could

be interpreted as a rapid mass transfer from the lower mass star to its companion. Supposing a conservative mass transfer, the quantity of mass transferred for this period change can be derived to be about $\Delta M = 2.45 \times 10^{-6} M_{\odot}$. The data located at $E > E_c$ show an oscillatory behavior around the second branch line. This variation has a period of $18.3 \pm 0.3 \text{ yr}$ in the $O - C$ diagram. Since this system does not seem to have significant magnetic activities, this cyclic trend could be attributed to the light-time effect caused by an invisible third body in the system. We obtain that the probability for the third body to be a low mass star with $M \geq 0.075 M_{\odot}$ is 5.4%. However, the third body has many more chances to be a brown dwarf with a probability of 94.6%. Supposing $i' = 90^{\circ}$, the semi-major axis of the third body becomes $a_3 = 8.04 \pm 0.33 \text{ AU}$, which is considerably larger than the common envelope of the binary. This system should be followed up by other future observations and more times of minima to reveal the nature of orbital period variations and our detected cycle in it. Hence these models can be considered as speculations for future reference.

We specified the photometric solution of the short period system BF Pav based on the Wilson-Devinney code combined with the MC simulation to calculate the uncertainties of the searched parameters. We obtained a mass ratio ($q = \frac{M_2}{M_1}$) of 1.460 ± 0.014 from the q-search method which suggested that BF Pav is a contact binary with a fillout factor (f) and an inclination (Table 3). Also, the difference between this binary system components' temperature ΔT is on the order of 200 K. We calculated the binary system distance which equals $268 \pm 18 \text{ pc}$ and this result is in good agreement with the Gaia Early Data Release 3 (EDR3) value $253.272 \pm 0.992 \text{ pc}$.

Based on the estimation of absolute parameters, the diagrams of Mass-Luminosity ($M-L$) and Mass-Radius ($M-R$) on a log-scale show the evolutionary status of BF Pav. The theoretical zero-age main sequence (ZAMS) and terminal-age main sequence (TAMS) lines and the positions of the primary and secondary components are depicted in Figure 6. Since the W UMa-type eclipsing binaries are known as Low-Temperature Contact Binaries (LTCBs), the difference between the temperatures of two components is close to each other and typically around 5%; this is about 4% for BF Pav. As discussed by Yakut & Eggleton (2005), in this type of contact binary system the luminosity of some primary is transferred to the secondary because of their initial masses. Moreover, in W UMa-type eclipsing binaries the components share a CCE, so the primary component is near the ZAMS (Fig. 6(a)). This is taken to mean that the primary is not yet evolved. Alternatively, the deviation of the secondary component shows it is slightly evolved from ZAMS. The secondary

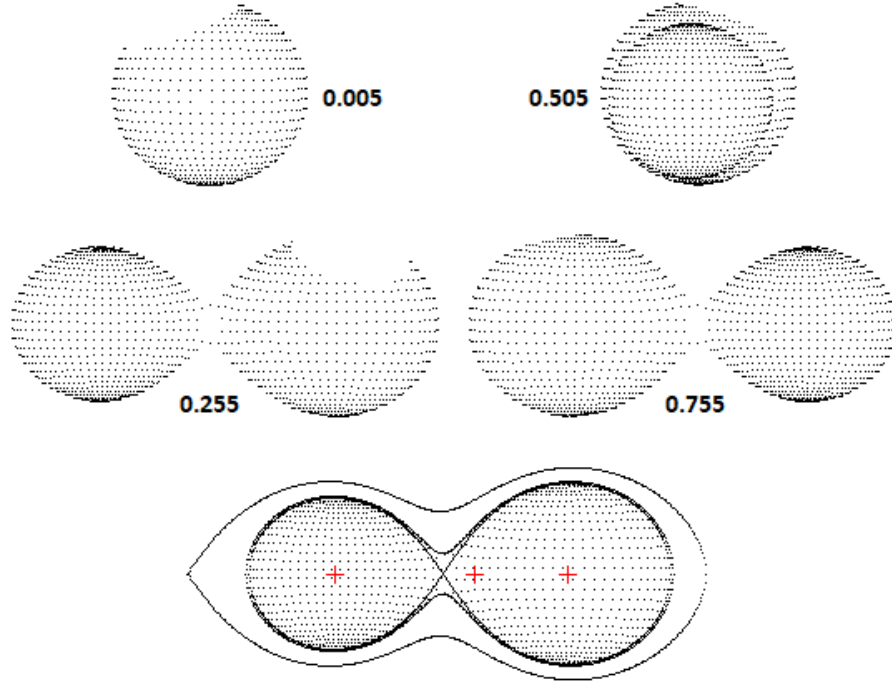


Fig. 5 The positions of the components of BF Pav.

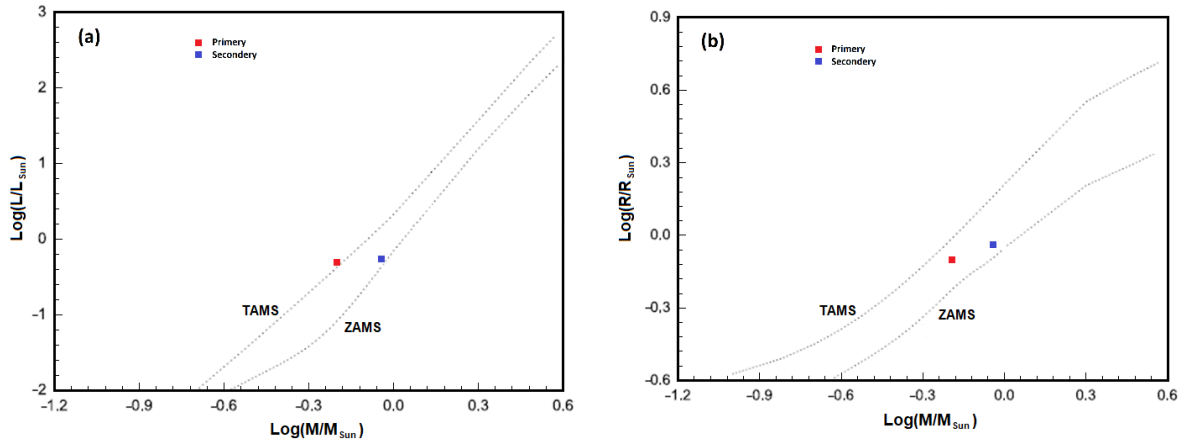


Fig. 6 The $\log M - \log L$ and $\log M - \log R$ diagrams for BF Pav from the absolute parameters. The dashed lines represent the TAMS and ZAMS and the locations of the primary and secondary components of BF Pav are marked.

components display different evolutionary paths due to more initial masses than the present masses (Yildiz & Doğan 2013). According to the value of the mass ratio, the fillout factor, which agrees with Gonzalez et al. (1996), we suggest that BF Pav is a W-type system. Yildiz & Doğan (2013) investigated the parameters of W-type W UMa binaries to estimate initial masses of these stars which were obtained based on MESA models (Paxton et al. 2011) due to mass transfer between two components. According to the mass loss model of Yildiz & Doğan (2013) and clearly from Figure 6, on the $\log M - \log L$ diagram, the location of both components of BF Pav appears to be in good

agreement with the distribution of primary and secondary stars of the W-type W UMa binary systems.

Stellar winds are the major mechanism responsible for a binary system's mass loss due to the star's magnetic activities. According to Table 4 and maximal differences in the light curves, it seems that BF Pav does not have significant magnetic activity and this implies a negligible O'Connell effect in this binary system and we concluded that the mass loss idea is not applicable for this system, so we concentrate on mass transfer.

BF Pav had been observed by Hoffmann (1981) but the observer has not been able to produce a detailed

analysis due to lack of data. Subsequently, the first detailed photometric analysis of BF Pav was performed in 1996 applying the Wilson-Devinney code (Gonzalez et al. 1996) after *UBV* photoelectric observations of this binary system were acquired between 1987 and 1993 in the observational program of southern short-period eclipsing binaries. The former photometric solution demonstrates that BF Pav has a mass ratio of 1.4 while we calculated $q = 1.460 \pm 0.014$. To complete our comparison, we found 12.5% for the amount of fillout factor whereas 10% was obtained for f in the prior study.

Acknowledgements This manuscript is based on the Binary Systems of South and North Project (<http://bsnp.info>). The project aims to study contact binary systems in the northern and southern hemispheres of several observatories in different countries.

References

- Applegate, J. H. 1992, *ApJ*, 385, 621
- Ballesteros, F. J. 2012, *EPL (Europhysics Letters)*, 97, 34008
- Bradstreet, D. H. 2005, *Society for Astronomical Sciences Annual Symposium*, 24, 23
- Code, A. D., Bless, R. C., Davis, J., & Brown, R. H. 1976, *ApJ*, 203, 417
- Collins, K. A., Kielkopf, J. F., Stassun, K. G., & Hessman, F. V. 2017, *AJ*, 153, 77
- Davoudi, F., Jafarzadeh, S. J., Poro, A., et al. 2020, *New Astron.*, 76, 101305
- Dryomova, G. N., & Svechnikov, M. A. 2006, *Astrophysics*, 49, 358
- Eker, Z., Bakış, V., Bilir, S., et al. 2018, *MNRAS*, 479, 5491
- George, D. B. 2000, *International Amateur-Professional Photoelectric Photometry Communications*, 79, 2
- Gonzalez, J. F., Lapasset, E., Gomez, M., & Ahumada, J. 1996, *PASP*, 108, 338
- Harmanec, P. 1988, *Bulletin of the Astronomical Institutes of Czechoslovakia*, 39, 329
- Hoffmann, M. 1981, *Information Bulletin on Variable Stars*, 1935, 1
- Høg, E., Fabricius, C., Makarov, V. V., et al. 2000, *A&A*, 357, 367
- Irwin, J. B. 1952, *ApJ*, 116, 211
- Juryšek, J., Hoňková, K., Šmelcer, L., et al. 2017, *Open European Journal on Variable Stars*, 179, 1
- Kreiner, J. M. 2004, *Acta Astronomica*, 54, 207
- Kwee, K. K., & van Woerden, H. 1956, *Bull. Astron. Inst. Netherlands*, 12, 327
- Lucy, L. B. 1967, *ZAp*, 65, 89
- Lucy, L. B., & Wilson, R. E. 1979, *ApJ*, 231, 502
- Mochnecki, S. W., & Doughty, N. A. 1972, *MNRAS*, 156, 51
- Negu, S. H., & Tessema, S. B. 2015, *International Journal of Astronomy and Astrophysics*, 5, 222
- O’Connell, D. J. K. 1951, *Publications of the Riverview College Observatory*, 2, 85
- Okamoto, I., & Sato, K. 1970, *PASJ*, 22, 317
- Paxton, B., Bildsten, L., Dotter, A., et al. 2011, *ApJS*, 192, 3
- Poro, A., Zamanpour, S., Hashemi, M., et al. 2021, *New Astron.*, 86, 101571
- Qian, S. B., Zhang, J., He, J. J., et al. 2018, *ApJS*, 235, 5
- Ruciński, S. M. 1969, *Acta Astronomica*, 19, 245
- Rucinski, S. M., Pych, W., Ogłóza, W., et al. 2005, *AJ*, 130, 767
- Schlafly, E. F., & Finkbeiner, D. P. 2011, *ApJ*, 737, 103
- Sekiguchi, M., & Fukugita, M. 2000, *AJ*, 120, 1072
- Shapley, H., & Mohr, J. 1940, *Annals of Harvard College Observatory*, 90, 239
- Smith, R. C. 1984, *QJRAS*, 25, 405
- Spencer Jones, J. H. 1988, *Information Bulletin on Variable Stars*, 3265, 1
- Stępień, K. 2006, *Ap&SS*, 304, 81
- Sung, H., Lim, B., Bessell, M. S., et al. 2013, *Journal of Korean Astronomical Society*, 46, 103
- van Hamme, W. 1993, *AJ*, 106, 2096
- Wilson, R. E., & Devinney, E. J. 1971, *ApJ*, 166, 605
- Yakut, K., & Eggleton, P. P. 2005, *ApJ*, 629, 1055
- Yang, Y.-G., & Qian, S.-B. 2015, *AJ*, 150, 69
- Yildiz, M., & Doğan, T. 2013, *MNRAS*, 430, 2029
- Zhang, L., Pi, Q., Han, X. L., et al. 2015, *New Astron.*, 38, 50
- Zola, S., Gazeas, K., Kreiner, J. M., et al. 2010, *MNRAS*, 408, 464
- Zola, S., Rucinski, S. M., Baran, A., et al. 2004, *Acta Astronomica*, 54, 299